Letter

Coupling Atmospheric and Biological Remote Sensing to Investigate Boundary-Layer Evolution and Animal Flight Behavior as Affected by the 2017 North American Solar Eclipse

Phillip M. Stepanian * and **Charlotte E. Wainwright**

Department of Civil and Environmental Engineering and Earth Sciences, University of Notre Dame, Notre Dame, IN 46556, USA; cwainwri@nd.edu
* Correspondence: p.step@nd.edu

check for updates

Abstract: The daytime atmospheric boundary layer is characterized by vertical convective motions that are driven by solar radiation. Lift provided by thermal updrafts is sufficiently ubiquitous that some diurnal birds and arthropods have evolved specialized flight behaviors to soar or embed in these atmospheric currents. While the diel periodicity of boundary-layer dynamics and animal flight has been characterized, rare disruptions to this cycle provide a chance to investigate animal behavioral responses to boundary layer motion and photoperiod that are disjointed from their expected circadian rhythm. To analyze these interactions, we couple radar-derived animal observations with co-located lidar measurements of the convective boundary layer over north-central Oklahoma, USA during the solar eclipse of 21 August 2017. Analysis of animal flight behavior confirmed that ascending and descending flight effort did change in the time period encompassing the solar eclipse, however, the response in behavior was coincident with proximate changes in boundary-layer turbulence. Both the animal behavioral response and decrease in atmospheric turbulence lagged changes in solar irradiance by approximately 30 min, suggesting that changes in flight activity were not cued by the eclipse directly, but rather by the modification of vertical air motions caused by the eclipse.

Keywords: aeroecology; biometeorology; lidar; radar

1. Introduction

Earth's atmospheric boundary layer is defined as the layer of air in contact with the ground, which has properties—dynamic, thermodynamic, or chemical—affected by the surface [1]. With the exception of aquatic and subterranean organisms, most animal life on Earth resides in the atmospheric boundary layer. While some of these terrestrial organisms spend their entire lives on the surface and experience only the lowest few meters of the boundary layer, many have evolved the capacity to move through the atmosphere using active locomotion or passive transport [2]. For these volant animals, it is challenging to investigate their aerial behavior without also understanding the atmospheric flow in which they are navigating [3–5].

During a cloud-free day over land, the atmospheric boundary layer is characterized by thermal convection resulting from surface radiative heating from the sun [1]. This convective boundary layer promotes vertical fluxes of momentum, energy, and mass, enabling upward transport of surface-based water vapor, aerosols, particulates, and organisms [1]. Persistent lift provided by thermals within the convective boundary layer enables vertical ascent and long-range dispersal by organisms that would otherwise be incapable of such movements (e.g., aphids [6] and ballooning spiders [7]) and extends flight

range for soaring animals (e.g., butterflies [8] and raptors [9]). Beyond driving atmospheric convection, sunlight also provides optical cues to organisms that can coincide with specific twilight behaviors (e.g., initiation and termination of flight, roost exodus and returns, calling by birds and insects [10,11], ascending flights by swifts [12]). Further complicating these interactions, many animals also have an endogenous circadian clock that also promotes daily behavioral periodicity (e.g., [13]). Overall, decoupling the behavioral effects stemming from diurnal boundary-layer evolution, photoperiod cues, and circadian rhythm is inherently challenging.

A total solar eclipse presents a unique case for potentially disentangling these effects by rapidly simulating twilight levels of incoming solar radiation at a novel time in the diel cycle. Previous work investigated aerial animal abundance at continental scales during the North American solar eclipse of 2017, reporting changes in altitudinal distributions and overall animal numbers aloft associated with passage of the eclipse [14]. These behaviors were attributed to light cues that evoked the familiar twilight roosting responses of diurnally active animals [14]. A meteorological study of this same event analyzed the effect of the eclipse on boundary-layer evolution, focusing on the land–atmosphere responses to rapid changes in radiative forcing [15]. Atmospheric measurements during the eclipse indicated a rapid halt to vertical motions, collapse of the convective boundary layer, and descent and decrease of water vapor concentrations aloft [15]. Interestingly, the spatiotemporal patterns found in aerosol and water vapor concentrations—passive tracers of boundary-layer structure—broadly match changes in aerial animal abundance and altitudinal distributions during the eclipse, potentially suggesting a coupled effect between animal flight behavior and boundary-layer dynamics. As a result, the effect of the eclipse on animal flight behavior—or lack thereof—is ambiguous, and requires additional analysis to determine whether animals are actively responding to optical cues or mirroring ambient boundary-layer structure.

Decoupling animal flight behavior from underlying boundary-layer dynamics requires simultaneous, co-located measurements of both animal and atmospheric motions. Collecting such measurements, especially at the spatiotemporal scales necessary to resolve the effect of an eclipse, is generally prohibitive. Previous work has demonstrated that vertically-pointing Doppler cloud radars can observe altitudinal distributions and vertical motions of animals aloft, while vertically-pointing Doppler lidars can measure underlying atmospheric motions [16,17]. Coupling these independent measurements enables a direct assessment of animal responses to their proximate atmospheric surroundings, and can be used to determine flight behavior within the convective boundary layer [16]. While the combined infrastructure required for making these dual measurements is rare, the field site in north-central Oklahoma that has enabled prior work using this method [16,17] was also a location affected by the 2017 solar eclipse [15]. We use the combination of atmospheric remote sensing of vertical air motions and measurements of animal ascent and decent rates to determine whether flight activity changed over the period of the solar eclipse.

2. Materials and Methods

The U.S. Department of Energy's Atmospheric Radiation Measurement (ARM) central facility in the Southern Great Plains (SGP) maintains a Ka-band (8.6 mm wavelength) dual-polarized profiling cloud radar that is co-located with a vertically-pointing Doppler lidar (36.605°N, 97.486°W). Within the clear-air boundary layer, most signals obtained by the cloud radar are from flying organisms—primarily insects—embedded in atmospheric currents [18]. The resulting velocity measurements from the radar are therefore a sum of the atmospheric motions and animal locomotion (i.e., active flight effort or settling velocity) [16]. The Doppler lidar uses a narrow, near-infrared beam to observe the backscatter from atmospheric aerosols, which are assumed to be ideal passive tracers of atmospheric motions [16]. By subtracting the lidar-derived wind velocity from the radar-derived total velocity, the animal flight velocity can be deduced [16].

We focus on one diel cycle encompassing the period of the solar eclipse on 21 August 2017, starting at local midnight (00:00 Central Daylight Time; 05:00 UTC) and ending 24 h later (23:59 CDT; 04:59

UTC). Radar observations are made at a period of approximately 3.7 s, and lidar observations are made at 1.54 s. The radar and lidar height bins are both at a spacing of 30 m, although the height intervals are not collocated. These two data streams are fused by linearly interpolating the lidar observations in time and height to correspond with the radar time and heights bins. The radar observations are filtered to isolate single animal scatterers by removing background noise (signal-to-noise ratio (SNR) <= −10 dB) and multiple scatterers in the beam (spectrum width >= 0.1 m s^{-1}) following [16]. The Doppler lidar data are similarly filtered to remove background noise using an SNR threshold of >= −21 dB following [15] (Figure 1).
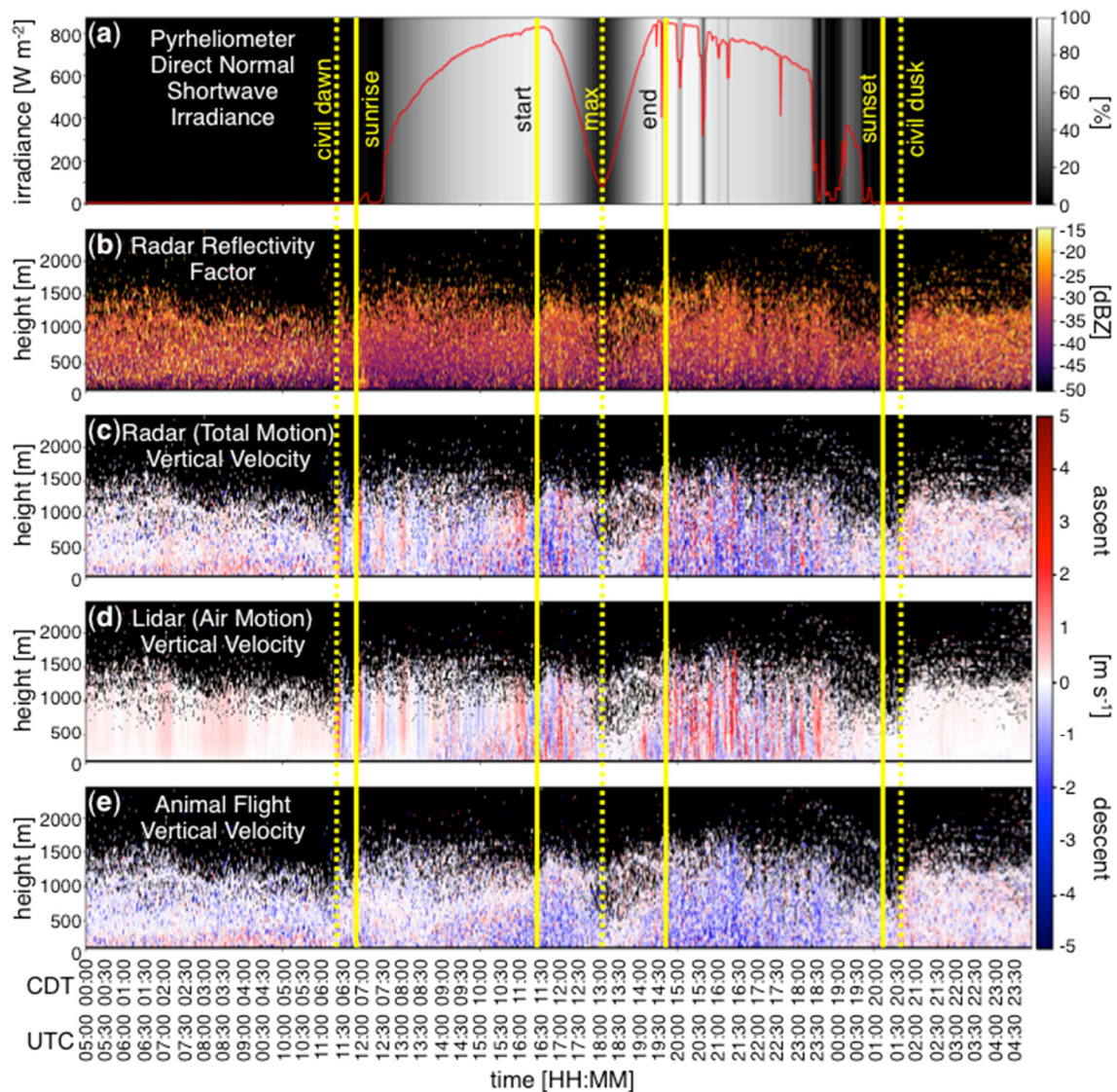

Figure 1. Time evolution of the solar eclipse, boundary-layer structure, and animal flight activity on 21 August 2017 at the ARM SGP site. (**a**) Direct normal shortwave irradiance (i.e., solar radiation) measurements from the pyrheliometer (red), and the percent of maximum expected noontime irradiance (gray scale shading); (**b**) Radar reflectivity factor, a measure of aerial animal abundance, as a function of time and altitude above ground level; (**c**) Radar-derived vertical velocity of animals including both contributions from active flight and atmospheric motions; (**d**) Lidar-derived atmospheric vertical velocity; and (**e**) Animal vertical flight velocity obtained by subtracting (**d**) from (**c**). In (**c**–**e**), blue shades indicate downward motions (descent) and red shades indicate upward motions (ascent). Vertical yellow bars denote times of civil twilight, sunrise, and sunset, as well as the start, maximum, and end of the eclipse period.

We compute relative frequency histograms of vertical wind and animal flight velocity by binning velocity measurements in 0.1 m s^{-1} increments at all altitudes within a 2-minute period and normalizing by the total number of observations (Figure 2). We also compute the variance of velocities within these 2-minute windows as a measure of turbulence (i.e., spatiotemporal wind velocity variance) and flight behavior (spatiotemporal flight effort variability), and apply a 10-point (i.e., 20-minute) running mean to aid visualization (Figure 3).
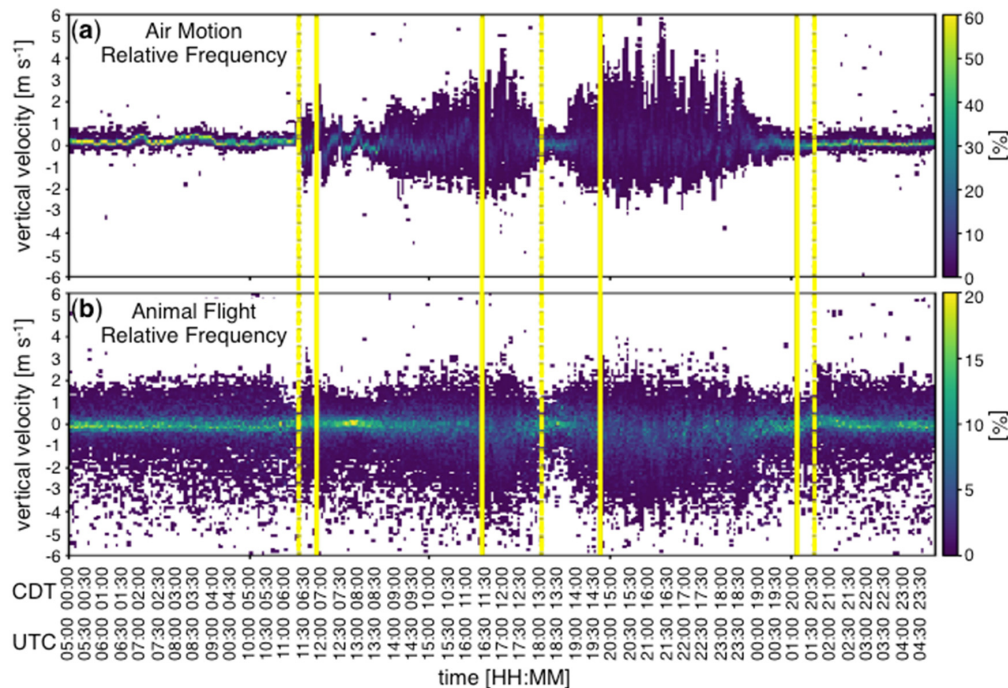

Figure 2. Time evolution of boundary-layer vertical motions and animal flight behavior. Two-minute relative frequency distributions of (**a**) atmospheric vertical motions, and (**b**) animal flight velocity (note that colorscale varies between **a** and **b**). Positive velocities indicate ascent and negative velocities indicate descent. Vertical yellow bars denote (left to right) onset of civil twilight, sunrise, start of eclipse, maximum eclipse, end of eclipse, sunset and end of civil twilight, as defined in Figure 1.
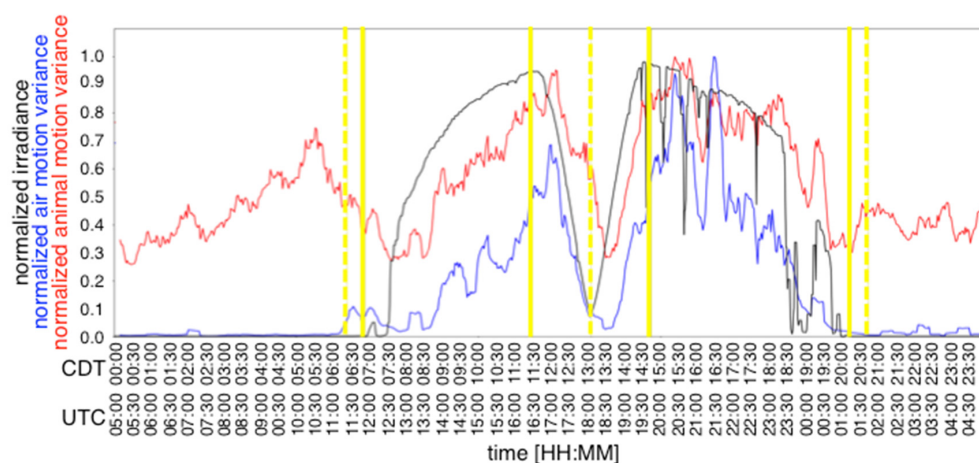

Figure 3. Time evolution of solar irradiance (black), boundary-layer vertical velocity variance (i.e., turbulence; blue), and animal flight effort variance (i.e., behavior; red). All three time series have been normalized to aid visual comparison. Vertical yellow bars denote (left to right) onset of civil twilight, sunrise, start of eclipse, maximum eclipse, end of eclipse, sunset and end of civil twilight, as defined in Figure 1.

To quantify the impact of the eclipse on downwelling radiation, we used Solar and Infrared Radiation Station (SIRS) pyrheliometer measurements of direct normal shortwave irradiance at the central facility (Figure 1). As a reference value, we calculated the expected maximum noontime irradiance in the absence of clouds or the eclipse by finding the maximum direct normal shortwave irradiance over the preceding four days (17–20 August). We defined the eclipse start as the time during the day when irradiance first begins to decrease and the eclipse maximum as the time during the eclipse when irradiance reaches its minimum. The eclipse end was defined as the time duration from eclipse start to maximum, added to the time of the eclipse maximum.

Finally, we computed cross correlation functions between time-series pairs of turbulence, animal behavior, and light level across a range of time lags to determine which pairs have the most coordinated responses (Figure 4). We made the assumption that animals will respond most immediately to the environmental forcing that is influencing their behavior, and as a result, the environmental forcing with the lowest temporal lag is assumed to be the behavioral driver.
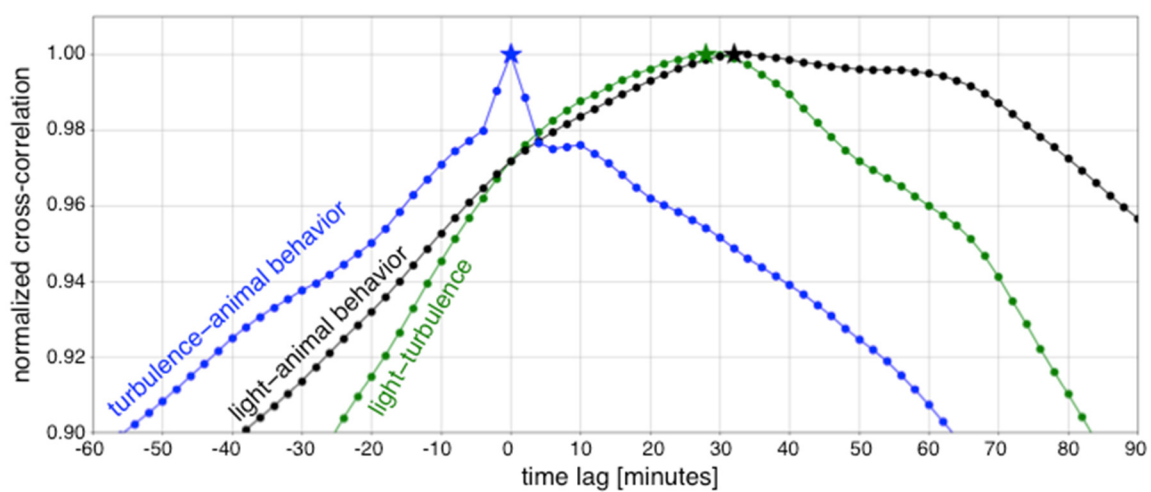

Figure 4. Normalized cross-correlation functions of turbulence and animal behavior (blue), light level and animal behavior (black), and light level and turbulence (green). The maximum cross correlation value of each pair is indicated by a star.

All data used in this study are open access and available for download at the ARM data center [19,20].

3. Results

The diel period on 21 August 2017 initially exhibited typical solar patterns, with the onset of civil twilight occurring at 06:24 CDT and sunrise at 06:52 CDT (Figure 1a). Clear-sky irradiance would typically continue to increase monotonically until the time of solar noon (13:33 CDT), however, at 11:28 CDT irradiance began to decrease as the sun began to be obscured. As solar obscuration continued to increase, irradiance decreased until it reached a minimum at 13:06 CDT, marking the eclipse maximum (Figure 1a) as solar obscuration reached 89%. Subsequently irradiance began to increase with the major direct effects of the eclipse on irradiance ending around 14:44 CDT. Short periods of broken clouds continued through the afternoon until sunset at 20:13 CDT and the end of civil twilight at 20:42 CDT (Figure 1a).

Radar reflectivity factor indicates widespread animal activity within the lowest 1.5 km throughout the diel period (Figure 1b), and radar vertical velocity shows variable ascent and descent rates throughout the day, with stronger vertical motions during the daytime convective boundary layer prior to and following the eclipse (Figure 1c). These patterns are more evident in lidar vertical velocity, illustrating the transition of the stable nocturnal boundary layer to the convective boundary layer

following sunrise. Similarly, the descent of the boundary-layer height, termination of convection, and return to stable conditions can be seen during the period of the eclipse (Figure 1d). A similar parallel can be seen in animal flight activity, with distinctly different behavior during the nocturnal period than in the daytime boundary layer, and eclipse behavior more closely mirroring flight in the nocturnal stable boundary layer (Figure 1e).

Relative frequency distributions of ascent and descent rates can further characterize time-varying changes in vertical motions through the diel cycle (Figure 2). Distributions of air velocities show little motion prior to sunrise, with convective intensity increasing through the morning (Figure 2a). Convective updrafts and downdrafts weaken as the eclipse progresses, and subsequently strengthen as the eclipse maximum passes (Figure 2a). As solar irradiance decreases into the evening, convection weakens until the boundary layer returns to a stable state following sunset (Figure 2a). Nocturnal animal flight demonstrates greater magnitude and variability in vertical motions than the stable atmosphere in which they are flying (Figure 2b). Throughout the day, the magnitude of animal ascent and descent rates largely follows the magnitude of vertical air motions of the convective boundary layer (Figure 2b). Most notable, as the boundary layer stabilizes during the peak of the eclipse, animal vertical motions weaken. Similarly, as the convective boundary layer redevelops following the eclipse, animal vertical motions increase in magnitude (Figure 2b).

To investigate the timing of variability in boundary-layer convection (i.e., turbulence) and animal flight behavior, we can calculate the vertical velocity variance for air and animal motions (Figure 3). It is clear that sunrise, sunset, and the eclipse all coincide with a clear change in the variability of atmospheric and animal vertical motions. Cross-correlation analysis of these three time series shows that changes in turbulence and animal flight behavior occur simultaneously, while changes in both turbulence and animal flight behavior lag changes in light level by approximately 30 min (Figure 4).

4. Discussion

Previous studies over this site in Oklahoma have shown that animals display variable flight behavior in response to boundary-layer stability (e.g., the nocturnal stable boundary layer versus the daytime convective boundary layer) and that flight effort is affected by the strength of convective updrafts and downdrafts [16]. An atmospheric study of the 2017 eclipse at this site reported that the eclipse initiated a rapid transition from a convective boundary layer to stable conditions representative of the nocturnal atmospheric environment [15]. This transition and its similarity to night-time conditions are most clear in time-varying distributions of vertical atmospheric motions (Figure 2a). Recalling that the vertical motions presented in Figures 1d and 2a are that of atmospheric aerosols, it is clear that even idealized passive tracers can exhibit apparent "behavior" in response to the eclipse—altitudinal descent and reduction in vertical motions—but these motions are exclusively an effect of changes in underlying boundary-layer dynamics. In this context, observations of animals that appear to respond to the eclipse (Figure 1c) have an ambiguity that their motions may indeed be behavioral responses or may be fully a result of atmospheric dynamics as in the case of passive tracers. By removing the atmospheric component of animal vertical motion (Figure 1e), we see that animal flight by active locomotion (i.e., flight effort) is affected by the solar eclipse (Figure 2b). Just as described in [14], the behavioral response was a descent in altitude and reduction in flight activity during the period of the eclipse.

Although a behavioral response was observed during the eclipse, the timing of these changes suggests a cue related to proximate boundary-layer dynamics rather than optical cues. We speculate the sequence of events occurs as follows. Prior to the onset of the eclipse, animals initially embed in convective thermals and follow the characteristic behaviors described in [16]. As solar obscuration begins, reductions in visible light have little effect on animal behavior, but weakening downwelling radiation begins to reduce surface heating. As surface heating weakens, surface air becomes less buoyant, instability weakens, convection becomes shallower, and vertical velocities slow. As the atmosphere stabilizes, convection ceases, and turbulence decreases; animals no longer need to react to

strong vertical atmospheric motions, and can assume less variable ascent and descent rates. As the sun first reappears, light levels begin to increase but animal behavior shows no immediate response. As downwelling radiation begins to heat the surface, the re-initiation of convection and subsequent growth of convective plumes evokes a behavioral response as animals must respond to vertical motions by modifying their ascent and descent rates. Assuming that animals prefer to maintain a given altitude, this behavior in the presence of vertical motions is similar to animal compensation flight behavior to horizontal wind drift—a strategy seen in birds [21], bats [22], and insects [23].

Overall, the delay of approximately 30 min between the initial decrease in solar radiation and the corresponding decreases in both turbulence and flight activity suggests that animals are responding to proximate convective intensity rather than decreasing light levels. A similar lag of approximately 30 min between the passage of the maximum eclipse (i.e., increase in solar radiation) and subsequent increases in turbulence and flight activity further support this explanation. The response of the atmospheric boundary layer to the solar eclipse at this site was investigated in detail by [15], and the timings of the changes in animal response reported herein correspond to the timing of the collapse and subsequent regrowth of the convective boundary layer.

5. Conclusions

Many volant animals—birds, bats, and insects—have adapted behaviors to make use of the typical cycle of the atmospheric boundary layer, such as using convective thermals to assist with energetically demanding uplift. Rare occurrences of a solar eclipse disrupt this cycle and offer a unique chance to investigate the effect of changing light levels on animal behavior. The North American solar eclipse on 21 August 2017 provided exactly such an opportunity. A recent study [14] used the US national weather radar network to show that varying light levels caused distinct changes in the altitudinal distribution and aerial density of animals aloft. Although weather radar data revealed changes in animal behavior coincident with the eclipse, without further instrumentation it was not possible to delineate whether animals in flight were responding directly to changing illumination levels, or to changes in the atmospheric boundary-layer structure induced by the cessation of turbulence following the removal of solar heating. By employing a collocated millimeter-wavelength cloud radar and a Doppler lidar, we are able to examine how both the atmospheric boundary layer itself and the volant animals embedded within it respond to the solar eclipse. Overall, we find that changes in animal response to atmospheric vertical motion lag changes in illumination by approximately 30 min, but exactly match changes in turbulence caused by the collapse of the convective boundary layer. As demonstrated in a previous study [15], the transition from convective to stable boundary-layer conditions lags declines in radiative forcing, and the redevelopment of convective structure does not occur until after maximum solar obscuration has already passed [15]. Our results suggest that the changes in animal flight behavior that occurred during the 21 August 2017 North American solar eclipse were caused not by the changing light levels directly but rather by the effect of the eclipse on boundary-layer dynamics; i.e., the animals' response was to changes in the flow field in which they were embedded, which were generated by the eclipse, rather than the visual cues of the eclipse itself. We suggest that coupling measurements of animal flight behavior and atmospheric dynamics provides a more complete picture of an animal's navigation strategy within its aerial habitat, and can elucidate the processes underlying observed flight behavior.

Conflicts of Interest: The authors declare no conflict of interest. The funders had no role in the design of the study; in the collection, analyses, or interpretation of data; in the writing of the manuscript, or in the decision to publish the results.

References

1. Stull, R.B. *An Introduction to Boundary Layer Meteorology*; Kluwer Academic: Dordrecht, The Netherlands, 1988; 670p.
2. Dudley, R.; Yanoviak, S.P. Animal aloft: The origins of aerial behavior and flight. *Integr. Comp. Biol.* **2011**, *51*, 926–936. [CrossRef] [PubMed]
3. Becciu, P.; Menz, M.H.; Aurbach, A.; Cabrera-Cruz, S.A.; Wainwright, C.E.; Scacco, M.; Ciach, M.; Pettersson, L.B.; Maggini, I.; Arroyo, G.M.; et al. Environmental effects on flying migrants revealed by radar. *Ecography* **2019**, *42*, 942–955. [CrossRef]
4. Shamoun-Baranes, J.; Liechti, F.; Vansteelant, W.M. Atmospheric conditions create freeways, detours and tailbacks for migrating birds. *J. Comp. Physiol. A* **2017**, *203*, 509–529. [CrossRef] [PubMed]
5. Chapman, J.W.; Klaassen, R.H.; Drake, V.A.; Fossette, S.; Hays, G.C.; Metcalfe, J.D.; Reynolds, A.M.; Reynolds, D.R.; Alerstam, T. Animal orientation strategies for movement in flows. *Curr. Biol.* **2011**, *21*, 861–870. [CrossRef] [PubMed]
6. Parry, H.R. Cereal aphid movement: General principles and simulation modelling. *Mov. Ecol.* **2013**, *1*, 1–15. [CrossRef] [PubMed]
7. Bell, J.R.; Bohan, D.A.; Shaw, E.M.; Weyman, G.S. Ballooning dispersal using silk: World fauna, phylogenies, genetics and models. *Bull. Entomol. Res.* **2005**, *95*, 69–114. [CrossRef] [PubMed]
8. Gibo, D.L.; Pallett, M.J. Soaring flight of monarch butterflies, *Danaus plexippus* (Lepidoptera: Danaidae), during the late summer migration in southern Ontario. *Can. J. Zool.* **1979**, *57*, 1393–1401. [CrossRef]
9. Duriez, O.; Kato, A.; Tromp, C.; Dell'Omo, G.; Vyssotski, A.L.; Sarrazin, F.; Ropert-Coudert, Y. How cheap is soaring flight in raptors? A preliminary investigation in freely-flying vultures. *PLoS ONE* **2014**, *9*, e84887. [CrossRef] [PubMed]
10. Bruni, A.; Mennill, D.J.; Foote, J.R. Dawn chorus start time variation in a temperate bird community: Relationships with seasonality, weather, and ambient light. *J. Ornithol.* **2014**, *155*, 877–890. [CrossRef]
11. Young, A.M. Temporal selection for communicatory optimization: The dawn-dusk chorus as an adaptation in tropical cicadas. *Am. Nat.* **1981**, *117*, 826–829. [CrossRef]
12. Hedenström, A.; Norevik, G.; Warfvinge, K.; Andersson, A.; Bäckman, J.; Åkesson, S. Annual 10-month aerial life phase in the common swift *Apus apus*. *Curr. Biol.* **2016**, *26*, 3066–3070. [CrossRef] [PubMed]
13. Moore, D. Honey bee circadian clocks: Behavioral control from individual workers to whole-colony rhythms. *J. Insect Physiol.* **2001**, *47*, 843–857. [CrossRef]
14. Nilsson, C.; Horton, K.G.; Dokter, A.M.; Van Doren, B.M.; Farnsworth, A. Aeroecology of a solar eclipse. *Biol. Lett.* **2018**, *14*, 20180485. [CrossRef] [PubMed]
15. Turner, D.D.; Wulfmeyer, V.; Behrendt, A.; Bonin, T.A.; Choukulkar, A.; Newsom, R.K.; Brewer, W.A.; Cook, D.R. Response of the land-atmosphere system over north-central Oklahoma during the 2017 eclipse. *Geophys. Res. Lett.* **2018**, *45*, 1668–1675. [CrossRef]
16. Wainwright, C.E.; Stepanian, P.M.; Reynolds, D.R.; Reynolds, A.M. The movement of small insects in the convective boundary layer: Linking patterns to processes. *Sci. Rep.* **2017**, *7*, 5438. [CrossRef] [PubMed]
17. Wainwright, C.E.; Reynolds, D.R.; Reynolds, A.M. Linking Small-Scale Flight Manoeuvers and Density Profiles to the Vertical Movement of Insects in the Nocturnal Stable Boundary Layer. *Sci. Rep.* **2020**, *10*, 1019. [CrossRef] [PubMed]
18. Chandra, A.S.; Kollias, P.; Giangrande, S.E.; Klein, S.A. Long-term observations of the convective boundary layer using insect radar returns at the SGP ARM climate research facility. *J. Climat.* **2010**, *23*, 5699–5714. [CrossRef]
19. Isom, B.; Lindenmaier, I.; Nelson, D.; Hardin, J.; Matthews, A.; Bharadwaj, N. Atmospheric Radiation Measurement (ARM). Available online: http://dx.doi.org/10.5439/1025218 (accessed on 13 November 2019).
20. Newsom, R.; Krishnamurthy, R. Atmospheric Radiation Measurement (ARM). Available online: http://dx.doi.org/10.5439/1374838 (accessed on 13 November 2019).

21. Bingman, V.P.; Able, K.P.; Kerlinger, P. Wind drift, compensation, and the use of landmarks by nocturnal bird migrants. *Anim. Behav.* **1982**, *30*, 49–53. [CrossRef]

22. Sapir, N.; Horvitz, N.; Dechmann, D.K.; Fahr, J.; Wikelski, M. Commuting fruit bats beneficially modulate their flight in relation to wind. *Proc. R. Soc. B Biol. Sci.* **2014**, *281*, 20140018. [CrossRef] [PubMed]

23. Chapman, J.W.; Nesbit, R.L.; Burgin, L.E.; Reynolds, D.R.; Smith, A.D.; Middleton, D.R.; Hill, J.K. Flight orientation behaviors promote optimal migration trajectories in high-flying insects. *Science* **2010**, *327*, 682–685. [CrossRef] [PubMed]